Journal of Alloys and Compounds 730 (2018) 408–416

Contents lists available at ScienceDirect

Journal of Alloys and Compounds

journal homepage: http://www.elsevier.com/locate/jalcom

# Effect of aluminum addition on the densification behavior and mechanical properties of synthesized high-purity nano-laminated $Ti_3SiC_2$ through spark plasma sintering

Alireza Pourebrahim [a, *], Hamidreza Baharvandi [a], Hamze Foratirad [b], Naser Ehsani [a]

[a] Faculty of Materials & Manufacturing Processes, Malek-Ashtar University of Technology, Tehran, Iran
[b] Materials and Fuel Research School, Nuclear Science and Technology Research Institute, Tehran, Iran

ARTICLE INFO

*Article history:*
Received 20 July 2017
Received in revised form
27 September 2017
Accepted 3 October 2017
Available online 4 October 2017

*Keywords:*
Nano-laminate $Ti_3SiC_2$
Aluminum
SPS
Purity
Mechanical property

ABSTRACT

To reveal the effect of Al content on the purity and mechanical properties of $Ti_3SiC_2$, the powder mixture of 1Ti/1.2Si/2TiC/xAl (x = 0–0.4) were sintered to synthesize $Ti_3SiC_2$ through spark plasma sintering (SPS). The sintering process was conducted at 1150 °C for 8 min under a pressure of 40 MPa. To evaluate the phase constituents and morphology of the sintered samples, X-ray diffraction and field emission scanning electron microscopy were used. It was found that addition of Al from 0.2 to 0.4 mol in the starting powder mixture led to synthesis of high-purity $Ti_3SiC_2$. Besides, with increasing the Al content in the starting powder mixture, the densification behavior of sintered samples was promoted. The results showed that the Vickers microhardness of high-purity samples became almost same at higher loads and moreover the measured Young's modulus ($E$) of the high-purity $Ti_3SiC_2$ samples were near to each other and increased with promoting the densification.

© 2017 Elsevier B.V. All rights reserved.

## 1. Introduction

Because of unusual combination properties of both metals and ceramics, $Ti_3SiC_2$ have been attracted a lot of attentions for recent years. $Ti_3SiC_2$ has better electrical and thermal conductivity than Ti and TiC and this ternary compound is elastically quite stiff with low density (4.52 g $cm^{-3}$). Its specific stiffness is comparable to that of $Si_3N_4$ and three times that of Ti. $Ti_3SiC_2$ is readily machinable, resistant to thermal shock and refractory. Also it is unusually damage tolerant which is caused by kink bands and different multiple energy-absorbing mechanisms such as diffuse micro-cracking, delamination, crack deflection, grain buckling, micro-cracking, delamination, crack deflection, grain buckling, grain pull-out, and grain push-out [1–5]. The amounts of hardness, Young's modulus and fracture toughness of $Ti_3SiC_2$, reported in the literatures are 4 GPa [1,3,6], 320–334 GPa [1,7,8] and 6 MPa $m^{1/2}$ [3], respectively. $Ti_3SiC_2$ is a likely candidate for structural applications at elevated temperatures, such as heating elements, turbine blades, stators and rotating electrical contacts like commutating brushes for AC motors [2].

Attempts to synthesize high-purity $Ti_3SiC_2$ bulk samples had been accompanied with the auxiliary phases such as TiC and SiC in the final samples, therefore synthesis of high-purity $Ti_3SiC_2$ used to be a great challenge [9]. Thence many researchers have been employed various methods to synthesize high-purity $Ti_3SiC_2$ in the form of bulk material such as HIP [10,11], hot pressing (HP) [12,13], infiltration [14–17], vacuum sintering [18] and spark plasma sintering (SPS) [19,20]. Among these techniques, the SPS method which is known as the pulse discharge sintering (PDS), is conducted at relatively low temperatures and short times with fine microstructure relative to others conventional methods. Due to the presence of plasma, the localized temperature was reported up to 10000 °C during spark plasma sintering process [21,22]. There are various starting powder mixtures in order to synthesize high-purity $Ti_3SiC_2$, Ti/Si/C [23–25], Ti/Si/TiC [19,24,26,27], Ti/SiC/C [24,28], Ti/SiC/TiC [29], Ti/$TiSi_2$/TiC [30], $TiH_2$/Si/TiC [31] and furthermore Si/TiC [32], which in turn these compositions have great effects on the amounts of secondary phases in the sintered samples. Moreover, in order to improve the content of $Ti_3SiC_2$ in the final product and lowering the synthesis temperature, addition of Al (it has low-melting temperature relative to another starting powders) was accomplished. Small addition of Al into the starting powder mixtures can improve the synthesis of $Ti_3SiC_2$ via forming an Al–Si alloy containing 0–44% Si at 1000 °C in the Al-C-Si-Ti

* Corresponding author.
*E-mail address:* Alirezapourebrahim.me@gmail.com (A. Pourebrahim).

https://doi.org/10.1016/j.jallcom.2017.10.018
0925-8388/© 2017 Elsevier B.V. All rights reserved.

quaternary system [20,26]. Zhou et al. [26] synthesized single-phase $Ti_3SiC_2$ by sintering starting powder mixture of 1Ti/1Si/2TiC/0.2Al at 1250–1300 °C. They reported that small variation of additional Al enabled TiC auxiliary phase formation. Ghosh et al. [33] fabricated nearly single-phase $Ti_3SiC_2$ and $Ti_3SiC_2$-TiC composites with the starting powder mixture of Ti/Si/TiC along with 0.2 mol Al at 1250 °C. They observed some bright agglomerates which were rich in Al. Zhang et al. [34] reported that optimum molar content of Al was in the range of 0.1–0.3 with starting powder mixture of Ti/Si/C and with increasing the Al content to 0.4, the TiC phase was formed again. As discussed above, in order to synthesize high-purity $Ti_3SiC_2$ ternary compound with the starting powder mixture of Ti/Si/TiC/Al, the optimum amount of Al was reported to be 0.2 mol. But recently, Gao et al. [35] synthesized $Ti_3(Al_{1-x}Si_x)C_2$ (x = 0–1) solid solution from starting powder mixture of Ti/Si/TiC/Al in the temperature range of 1500–1600 °C. The loss of density was reported with simultaneous increment of Al and reduction of Si contents in the starting powder mixtures. Besides, they reported uniform distribution of Ti, Si and Al elements in the microstructure. As seen, there are some different and complex results about the addition of Al contents.

In this study, to reveal the effect of Al content on the purity of $Ti_3SiC_2$, microstructure, lattice parameter, density and mechanical properties of prepared samples through SPS, the starting powder mixtures of 1Ti/1.2Si/2TiC/xAl (x = 0, 0.1, 0.2, 0.3 and 0.4) were sintered at 1150 °C for 8 min. In addition, the effect of different Al contents on high-temperature behavior (initiation and completion of densification process) of samples was investigated.

## 2. Materials and methods

Commercial powders of Ti (<40 μm, >99%), Si (2–5 μm, >98%), TiC (3–5 μm) and Al (130 μm, 99%) were used as the starting powders. The molar ratios of starting powders were selected to 1Ti/1.2Si/2TiC/xAl with x = 0, 0.1, 0.2, 0.3 and 0.4. In order to compensate the loss of Si at higher temperatures, off-stoichiometry molar content of Si were used. The powder mixtures were ball-milled at room temperature for 5 h using a planetary ball mill with WC jars and zirconia balls under argon protective atmosphere. The ball to powder ratio was set at 10:1 and the milling speed was 200 rpm. Then the ball-milled powders were filled in a cylindrical graphite mold (30 mm in diameter) and sintered in vacuum by using SPS apparatus. The starting applied pressure was set at 40 MPa and the heating rate is controlled about 20–25 °C.min$^{-1}$. The sintering temperature was maintained at 1150 °C for 8 min. The pyrometer used to measure the temperature in our study, was focused on the center of mold through a drilled hole on the upper graphite punch. The calibration method for measuring the temperature was drilling a hole on upper punch from the top surface to 5 mm at the end of punch. Two graphite layers (0.2 mm in thickness) were placed between the punches and samples. The samples labeled as A0, A0.1, A0.2, A0.3 and A0.4 for SPS sintered powder mixtures with Al contents of 0, 0.1, 0.2, 0.3 and 0.4, respectively. To study the sintering behavior of bulk samples, the displacement of the shifting upper ram of the SPS apparatus was recorded while the lower ram was fixed.

After sintering, the samples were ground to remove the graphite layer. Then the phase constitution identification were performed using X-ray diffraction (XRD) experiments by PHILIPS PW1730 using Cu-K$\alpha$ radiation at 30 kV and 40 mA and step size of 0.05°.s$^{-1}$. The quantification amounts of the formed phases along with the related lattice parameters were determined with the Rietveld refinement [36]. In addition to the Rietveld refinement, the quantification amounts of phases were calculated by the standard additive methods [27] as well to validate the results. The relative densities of samples were determined by Archimedes method according to ASTM B311-93 (2002) e1 standard. Subsequently, the samples were polished and etched by a solution of $H_2O$:$HNO_3$:HF (1:1:1) to expose the $Ti_3SiC_2$ grains. The morphology and microstructure of samples were observed and analyzed by using field emission scanning electron microscope (FE-SEM) equipped with energy dispersive spectroscopy (EDS). The Young's modulus of samples was measured by Pulse-Echo method, using ASTM E797-95. The Vickers hardness tests were performed at 0.5, 1, 3, 5 and 10 N loads with a dwelling time of 10 s and then in order to observe the damage zones and crack propagation from the corners of indentations, an optical microscope (OM) was employed. The values of Young's modulus and microhardness are the average of 5 measurements.

## 3. Result and discussion

### 3.1. X-ray diffraction patterns

Fig. 1 illustrates the XRD patterns of SPS sintered samples with different Al contents. It can be observed that with decreasing Al content lower than 0.2 mol (A0 and A0.1 samples), the synthesis of $Ti_3SiC_2$ has been found more difficult. When no Al content was used in the starting powder mixture, no $Ti_3SiC_2$ was formed in the SPS sintered sample (A0 sample). As seen in Fig. 1 (a), the main peaks of A0 sample were related to the Ti and SiC phases. The Si in the starting powder mixture was reacted to the graphite layer between powder and punch and therefore the SiC phase was formed. In addition to observed peaks, the TiC, $Ti_5Si_3$ and $TiSi_2$ peaks were identified. With the addition of Al content to 0.1 mol (A0.1 sample), the Ti, SiC and $TiSi_2$ peaks disappeared and the $Ti_3SiC_2$ peaks began to intensifying at $2\theta \approx 39.53°$ (Fig. 1 (b)). It is clearly seen that with addition of Al, the formation of intermediate $Ti_5Si_3$ phase was promoted which improved the $Ti_3SiC_2$ content in the sintered samples. With increasing Al content to 0.2, 0.3 and 0.4 mol (A0.2, A0.3 and A0.4 samples), as shown in Fig. 1 (c)-(e), all peaks were related to $Ti_3SiC_2$ with the main peak at $2\theta \approx 39.5°$ and no other secondary phases were identified. According to the XRD results, it is clearly seen that Al played a key role on the synthesis of $Ti_3SiC_2$ and decreasing the sintering temperature as well. As the Al content was decreased to zero or 0.1 mol, the sufficient sintering temperature for the synthesis of high-purity $Ti_3SiC_2$ was increased.

The weight percentage amounts of phases formed in the A0.1 sample, calculated by the Rietveld refinement and related profile agreement factor ($\chi^2$, goodness of fit) and standard additive method are presented in Table 1. As it can be seen, due to overlapping peaks in the diffraction patterns, the discrepancies of calculated weight percentage amounts were significantly high. In this situation, the Rietveld refinement is more acceptable, because of its capability to refine complicated and low symmetry structures with many overlapping peaks.

The lattice parameters and lattice volume of high-purity $Ti_3SiC_2$ samples, calculated with the Rietveld refinement, are presented in Table 2 along with profile agreement factor. As it can be observed, with decreasing Al content, the lattice volume of $Ti_3SiC_2$ slightly increased. The lattice parameters (a and c) were not changed significantly. These lattice parameters and lattice volumes are in good agreement with the ones reported by Gao et al. [35]. They expressed that with increasing the Si content in the starting powder mixture, the c-lattice parameters were decreased whereas no change was observed in the a-lattice parameters.

### 3.2. Microstructural analysis

To evaluate the effect of Al addition on the microstructure of

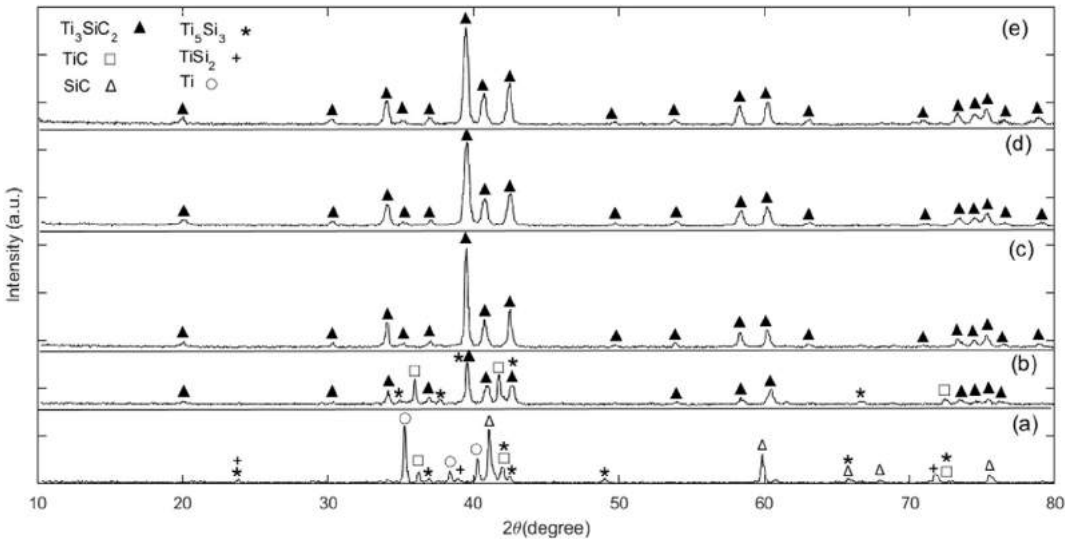


**Fig. 1.** XRD patterns of (a) A0, (b) A0.1, (c) A0.2, (d) A0.3 and (e) A0.4 samples.

**Table 1**
Weight percentage amounts of formed phases in the A0.1 samples with the Rietveld refinements and standard additive method.

| Sample | Rietveld Refinement | | | | Std. Add. Method | | |
|---|---|---|---|---|---|---|---|
| | $Ti_3SiC_2$(%) | TiC(%) | $Ti_5Si_3$(%) | $\chi^2$ | $Ti_3SiC_2$(%) | TiC(%) | $Ti_5Si_3$(%) |
| A0.1 | 30 | 31 | 39 | 4.39 | 62.34 | 18.4 | 19.26 |

**Table 2**
Summary of lattice parameters and lattice volume obtained from Rietveld refinements.

| Sample | Rietveld Refinement | | | | |
|---|---|---|---|---|---|
| | a = b(Å) | c(Å) | Lattice volume(Å) | c/a | $\chi^2$ |
| A0.2 | 3.068 | 17.678(2) | 144.1 | 5.7620 | 2.17791 |
| A0.3 | 3.068 | 17.677(2) | 144.09 | 5.7617 | 1.68330 |
| A0.4 | 3.066 | 17.679(3) | 143.92 | 5.7661 | 2.00547 |

Numbers in parentheses are estimated standard deviations in the Rietveld refinements.

high-purity samples, polished and etched surfaces of the A0.2, A0.3 and A0.4 samples were investigated by FE-SEM microscopy. As seen in Fig. 2, duplex microstructure of plate shaped grains and equiaxed grains were distinguished. With increasing the Al content, the length of plate shaped grains was incremented and the grain growth was occurred. The viscosity amounts of Al are presented as a function of temperature in Table 3. As seen, with increasing the temperature, the viscosity of liquid Al is decreased and reached from 1.298 mPa s at the melting point to 0.865 mPa s at the temperature of 927 °C [37]. It was expressed that increase in the Ti content provides an increase in the viscosity of liquid Al whereas with increasing the Si content, viscosity of liquid Al decreases [38]. Therefore, addition of Al could accelerate the diffusion of Ti and Si atoms and then promoted the synthesis of $Ti_3SiC_2$ at lower temperature. Liquid phase sintering may help distribute the current and heat more uniformly. As the liquid forms, the particle rearrangement and rotating can take place by the reduction of friction between the particles and the capillary forces of liquid as well. Consequently, there is a better densification relative to the solid state sintering [39,40]. In addition, more Al content led to more equiaxed grains. The length of plate shaped grains was reached to approximately 5 μm in the A0.3 and A0.4 samples. Based on the literature [20,26], the length and width of plate shaped grains of high-purity $Ti_3SiC_2$ samples could reach to 2–4 times greater than our results which is owing to higher sintering temperature. The effect of Al addition on the synthesis of $Ti_3SiC_2$ and solid solution of $Ti_3(Si_{1-x}Al_x)C_2$ was studied from the EDS mapping of Ti, Si and Al (white points) elements on the A0.2 and A0.3 samples which are indicated in Fig. 3. As seen, plate shaped grains had uniform distribution of Si and Ti which indicates formation of $Ti_3SiC_2$ in the sintered samples. Besides, un-uniform distribution and agglomeration of Al elements were observed throughout both samples which was slightly higher than in the A0.3 samples. As it can be seen, these Al elements were almost agglomerated in the equiaxed grains. According to the EDS results of A and B microzones, which are shown in Fig. 3, large plate shaped grains and equiaxed grains were attributed to the $Ti_3SiC_2$ and solid solution of $Ti_3(Si_{1-x}Al_x)C_2$, respectively. This is in a good agreement with the results of Ghosh et al. [41] which reported that the microzones analyzed by EDS experiments, including the intense Al peak and Ti and Si peaks, seems to be solid solution of $Ti_3SiC_2$ and Al.

Fig. 4 illustrates the backscatter electron FE-SEM micrograph of sample sintered with starting powder mixture of Ti:Si:TiC:Al = 1:1.2:2:0.1 at 1150 °C (A0.1 sample). According to the EDS results corresponding to C-G microzones, presented in the Table 4, it can be said that in addition to the $Ti_3SiC_2$, $Ti_5Si_3$ and TiC phases, which identified in the XRD patterns, some ternary and tetramerous compounds were observed. Thermodynamically, ternary compound can be referred to the TiC, SiC and C phases. Also, this ternary compound was located in the $Ti_5Si_3C_x$ phase. Therefore, it can be suggested that $Ti_5Si_3C_x$ could be formed with the reactions between TiC and SiC phases. As it can be observed in Fig. 4, $Ti_3SiC_2$ phase was formed in the common boundary of $Ti_5Si_3C_x$ and TiC phases and then this is a logical conclusion which formation of $Ti_3SiC_2$ was the result of $Ti_5Si_3C_x$ and TiC phases.

Nano-laminate nature of $Ti_3SiC_2$ present in the high-purity samples is shown in Fig. 5. It is clearly seen that these nano-layers were lied on the each other. The damage tolerant property of $Ti_3SiC_2$ is attributed to these nano-layered structures which can alternately deflect the crack fracture force in the inter-layer and consequently promote the fracture toughness. The arrows, specified in Fig. 5, are the representative of different plastic deformation mechanisms. The formation of kink bands and bending of nano-laminates are clearly observed which is indicative of high

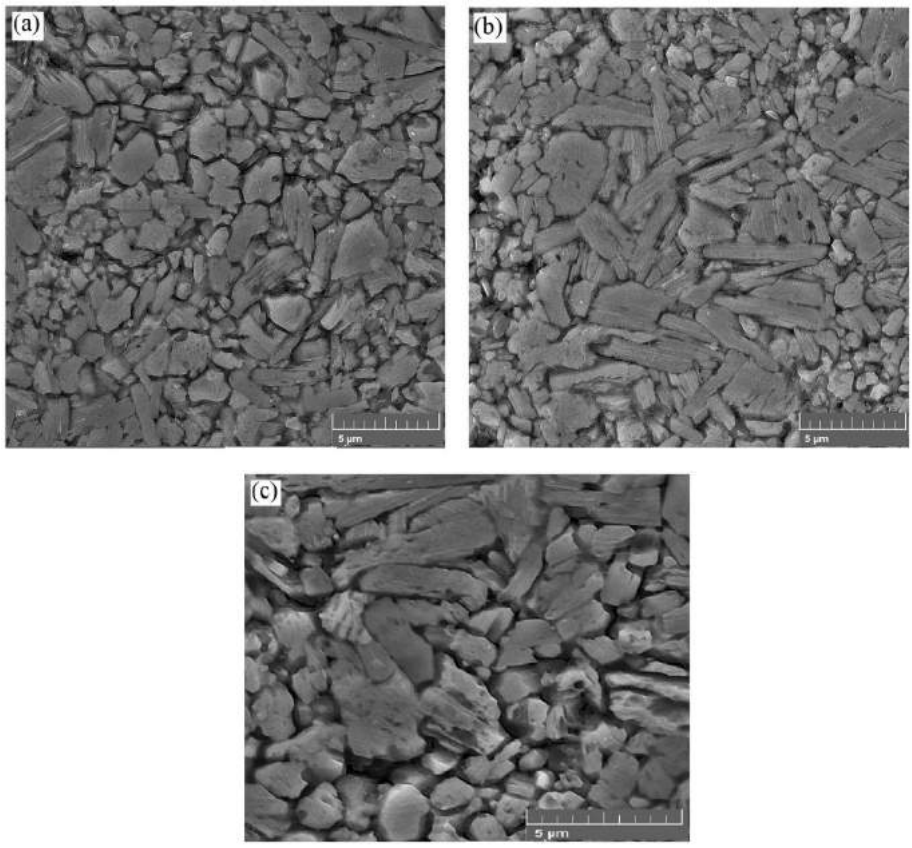


**Fig. 2.** Secondary electron FE-SEM micrographs of (a) A0.2, (b) A0.3 and (c) A0.4 samples.

**Table 3**
Viscosity amounts of Al as a function of temperature [37].

| Temperature (°C) | 677 | 702 | 727 | 752 | 777 | 802 | 827 | 852 | 877 | 902 | 927 |
|---|---|---|---|---|---|---|---|---|---|---|---|
| Viscosity (mPa.s) | 1.298 | 1.235 | 1.178 | 1.126 | 1.079 | 1.035 | 0.996 | 0.959 | 0.925 | 0.894 | 0.865 |

plasticity $Ti_3SiC_2$ at high temperature.

### 3.3. Sintering behavior and density

To study the sintering behavior of SPS sintered samples at high temperatures, the displacement curves as a function of time and temperature were used. Fig. 6 illustrates the sintering behavior of A0.4 sample at high temperatures. This displacement directly indicates the sintering shrinkage profile during densification of the compacts. As shown, there was two distinct points in the displacement curves which indicated the initiation (S point) and completion (F point) of densification process. The temperature of initiation and completion of densification process is listed in Table 5. It is apparent that the compact with maximum Al content, began to densify at lower temperature than those with 0.2 and 0.3 mol. The sintering shrinkage of A0.4 compact initiated at the temperature of 985 °C but with decreasing Al content to 0.3 and 0.2 mol, this temperature increased to 1017 °C and 1066 °C, respectively. The sintering shrinkage of A0.4 sample finished at the temperature of 1088 °C, while the shrinkage of A0.3 and A0.2 samples completed at the temperatures of 1112 and 1130 °C, respectively. It can be seen that the Al addition to the starting powder mixture decreased both initiation and completion temperatures of densification and resulted in ≈40 °C temperature difference between the initiation and completion temperatures of samples in compared to each other. These results clearly indicate the enhancing effect of Al content on the densification behavior of samples. Addition of Al was led to the formation of melting bath at ≈ 600 °C and subsequently, acceleration of Ti and Si diffusion in the compacts.

Fig. 7 shows the variation of density and relative density of samples sintered at 1150 °C for 8 min as a function of Al content. The relative densities of samples increased rapidly from 91.28% to 98%–98.5% with appropriate addition of Al. The relative densities of A0.2, A0.3 and A0.4 were 98.02%, 98.3% and 98.48%, respectively. With increasing Al content from 0.2 mol to 0.4, the relative densities enhanced slightly, which confirmed the displacement results at high temperatures. Moreover, the particle refinement induced by ball-milling process can lead to arrangement of atoms on the free surface and then fine particles have lower melting temperatures relative to larger ones [42]. Thermodynamically, sintering is an irreversible process which its driving force is decrease in free energy (through decrease in surface area) and then mass transport to the necking zone promotes with reduction of particle size. Decrease in the particle size provides an increment in the grain boundary and surface area and consequently free surface energy [43]. Therefore, with increasing the free surface energy due to increment of surface energy, sintering could take place at lower sintering temperature.

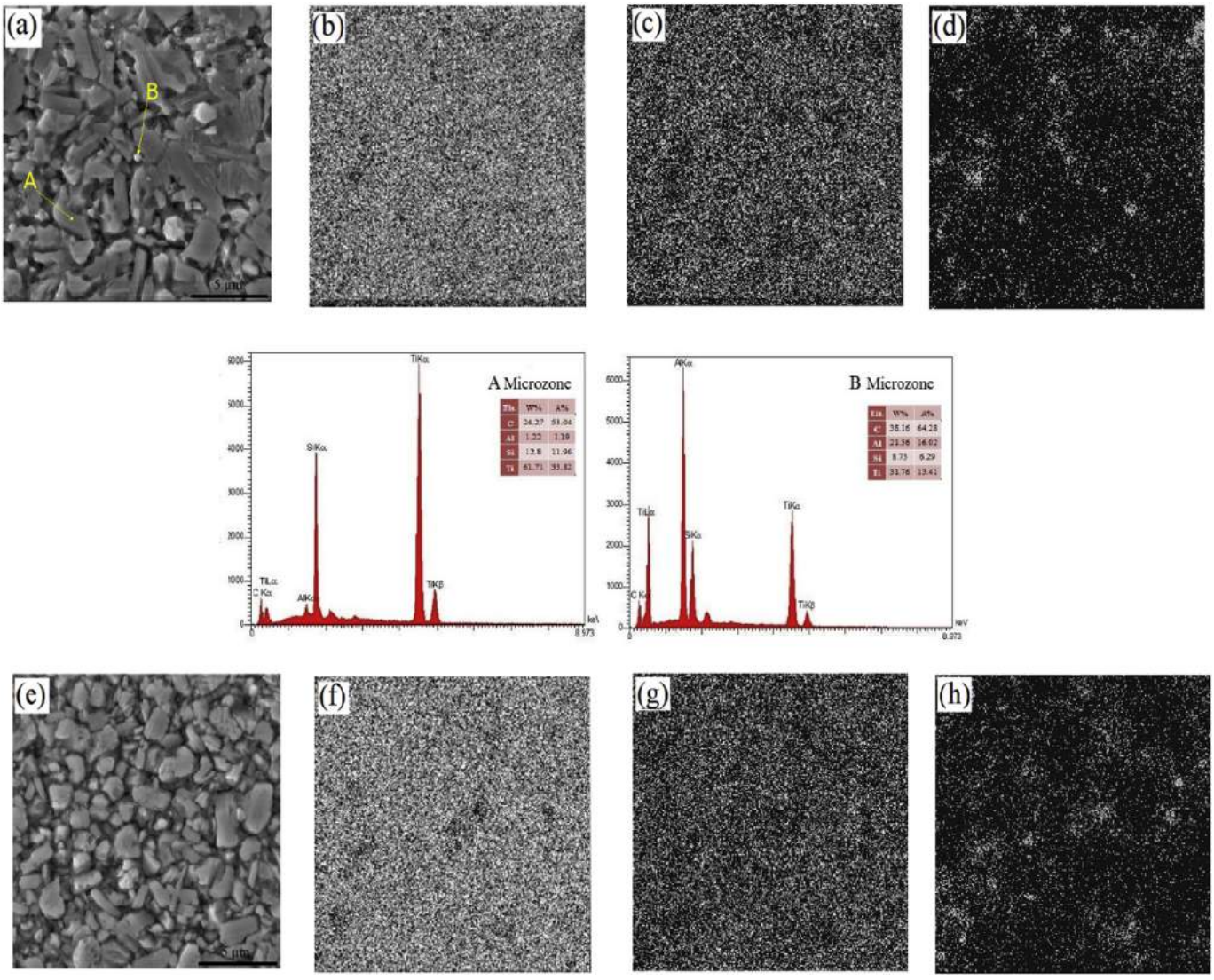


**Fig. 3.** Secondary electron FE-SEM micrographs and EDS mapping of Ti, Si and Al on the (a–d) A0.2 and (e–h) A0.3 samples, respectively.

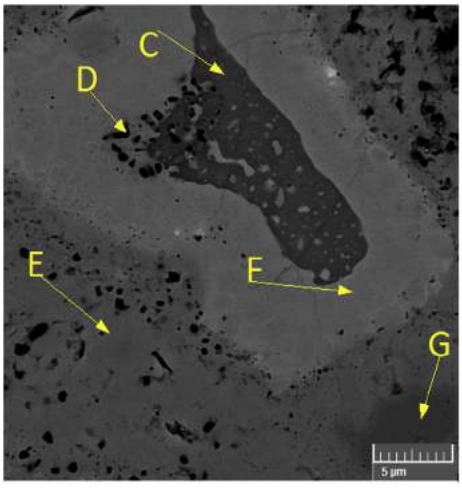


**Fig. 4.** Backscatter electron FE-SEM micrograph of A0.1 sample.

**Table 4**
EDS results from C-G microzones.

| Microzone | Composition (atomic percent) | | | | Possible phase |
|---|---|---|---|---|---|
| | Ti | Si | Al | C | |
| C | 12.78 | 20.81 | 2.48 | 63.92 | Ti-Si-C compound |
| D | 17.87 | 15.83 | 26.68 | 39.62 | Ti-Si-Al-C compound |
| E | 38.17 | 12.1 | 0.43 | 49.3 | $Ti_3SiC_2$ |
| F | 28.1 | 18.11 | 1.93 | 51.86 | $Ti_5Si_3C_x$ |
| G | 43.16 | 0.22 | 0.18 | 56.44 | TiC |

### 3.4. Mechanical properties

Fig. 8 (a)-(c) represent the Vickers microhardness of samples as a function of the applied indentation load. It can be observed that at lower loads, especially 0.5 N, the hardness values were high which represents the hardness of mono-crystal as indentation was within one grain. The Vickers microhardness of A0.2 sample was higher than two other samples at low indentation loads. This result

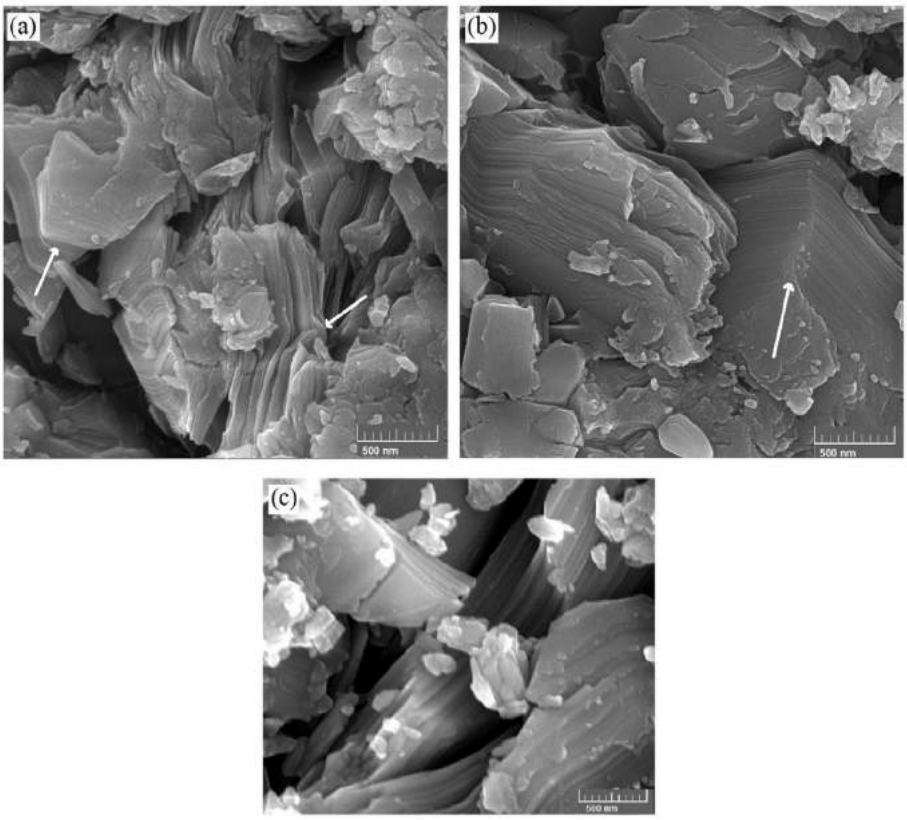


**Fig. 5.** FE-SEM micrographs of nano-laminated $Ti_3SiC_2$ in the (a) A0.2, (b) A0.3 and (c) A0.4 samples.

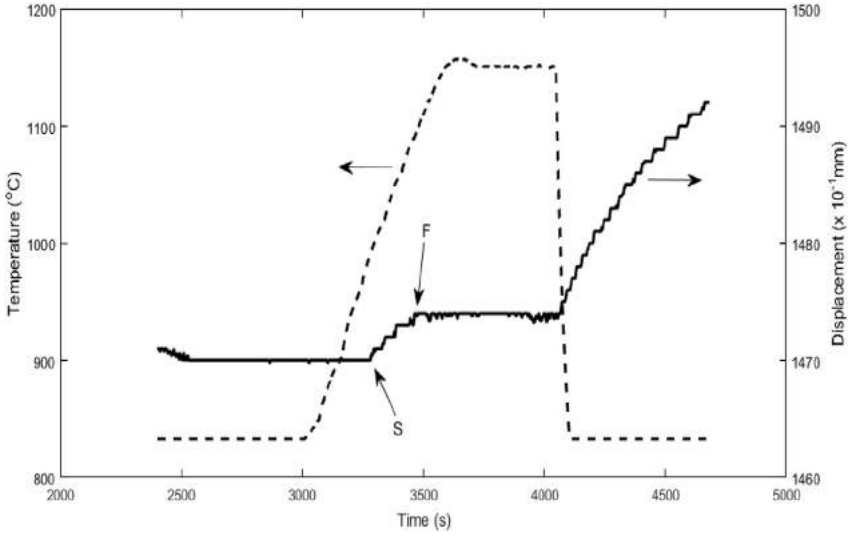


**Fig. 6.** Sintering behavior of A0.4 sample at high temperatures.

**Table 5**
Summary of densification process during spark plasma sintering of A0.2, A0.3 and A0.4 samples.

| Sample | Initiation Temperature(°C) | Completion Temperature(°C) | Transformation Time from S to F(s) |
|---|---|---|---|
| A0.2 | 1066 | 1130 | 145 |
| A0.3 | 1017 | 1112 | 190 |
| A0.4 | 985 | 1088 | 184 |

confirmed the finer microstructure of A0.2 sample which shown in the microstructure analysis section. Based on the Hall-Petch equation [44], as the grain size increases, the hardness decreases. Moreover, this decrease can be attributed to the Al content. Zhou et al. [45] reported that with addition of 0.25 mol Si to the ternary compound $Ti_3AlC_2$, the Vickers hardness was promoted but this was lower than that of $Ti_3SiC_2$. As discussed before, with increasing the Al content in the staring powder mixture, more equiaxed grains

were observed and it can be concluded that addition of 0.3 and 0.4 mol Al in the starting powder mixtures led to decreasing the microhardness relative to A0.2 sample at low loads. As indentation load increased, the hardness decreased for all samples and the microhardness values became independent of indentation load and grain size. The Vickers microhardness of A0.2, A0.3 and A0.4 samples at 10 N load were 6.94 ± 0.51 GPa, 6.78 ± 0.76 GPa and 6.85 ± 0.62 GPa, respectively. The obtained results are similar to each other and in a relatively good agreement with the value reported by Goto and Hirai (6 GPa) at 10 N [46]. In addition, Ghosh et al. [33] obtained a hardness value of 5.96 ± 0.19 GPa for the nearly single phase $Ti_3SiC_2$ at 10 N. The promoted Vickers microhardness obtained in the high-purity samples could be related to the solid solution hardening. Gao et al. [35] reported that the Vickers microhardness of $Ti_3SiC_2$ increased from 4.3 GPa at 10 N load to 5.2 GPa for solid solution of $Ti_3(Al_{1-x}Si_x)C_2$ with x = 0.4 at

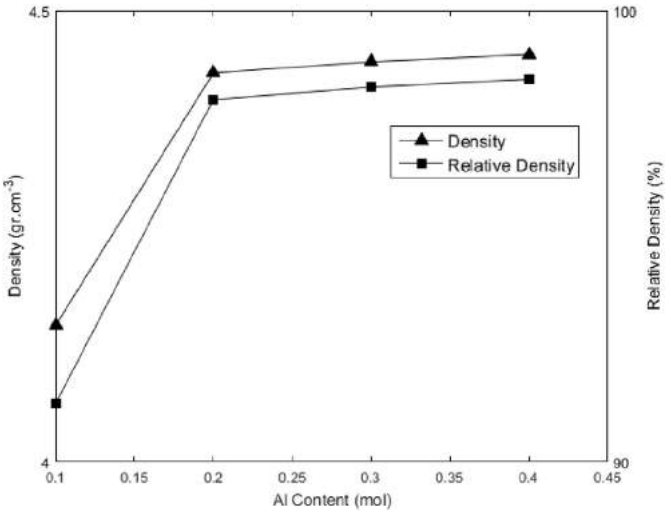


**Fig. 7.** Effect of Al content on the density of A0.1, A0.2, A0.3 and A0.4 samples, sintered at 1150 °C for 8 min.

the starting powder mixture. The Vickers microhardness of A0.1 sample obtained 8.18 ± 1.19 GPa at load of 2 N. The high standard deviation value observed in the A0.1 sample can be related to the hardness values of distinct components with high values related to the TiC (28–35 [47]) and low ones related to the pure $Ti_3SiC_2$. Abderrazak et al. [48] reported a hardness value of 9.37 GPa at 5 N load for a final product contained 57.9 wt% $Ti_3SiC_2$, 35.76 wt% TiC and 5.02 wt% $TiSi_2$.

Fig. 9 represents the optical micrographs of Vickers indentation conducted at 0.5, 5, 10 N on polished surface of A0.2 sample. It is clearly seen that at low indentation, no plastic deformation was carried out around the indentation mark, but with increasing the indentation load, the pile up of the material and damage were observed in the neighborhood of the indentation that normally occurs in the metals. When the indentation load was increased from 5 N to 10 N, the material piled up around the indentation mark, got more apparent. Also, no cracks were observed in the neighborhood of the indentation mark and the damage was confined to the immediate vicinity of the indentations.

Table 6 presents the longitudinal sound velocity ($V_l$) and the Young's modulus results of SPS sintered samples. It is apparent that the longitudinal sound velocity and Young's modulus increased with enhancing densification in the A0.2, A0.3 and A0.4 samples. The maximum amounts of longitudinal sound velocity and Young's modulus were attributed to the A0.4 sample which had maximum Al content among the samples and subsequently, the best densification behavior. These results confirmed the Rietveld refinement results. Gao et al. [35] expressed that with increasing Si content in the $Ti3(Al_{1-x}Si_x)C2$ solid solution, the Young's modulus was increased due to stronger M-A bonding. Since there were no significant variation between c-lattice parameters for high-purity $Ti_3SiC_2$ samples, then the related Young's modulus amounts were comparable to each other. The Young's modulus of high-purity $Ti_3SiC_2$ samples are in relatively good agreement with values that were obtained from pulse-echo method ($E$ = 353 GPa, $V_l = 9350\ m\ s^{-1}$) [49] and RUS results ($E = 343$ GPa, $V_l = 9185\ m\ s^{-1}$) [50]. With decreasing the Al content to 0.1 mol (A0.1 sample) and subsequently increasing the secondary phases, the longitudinal

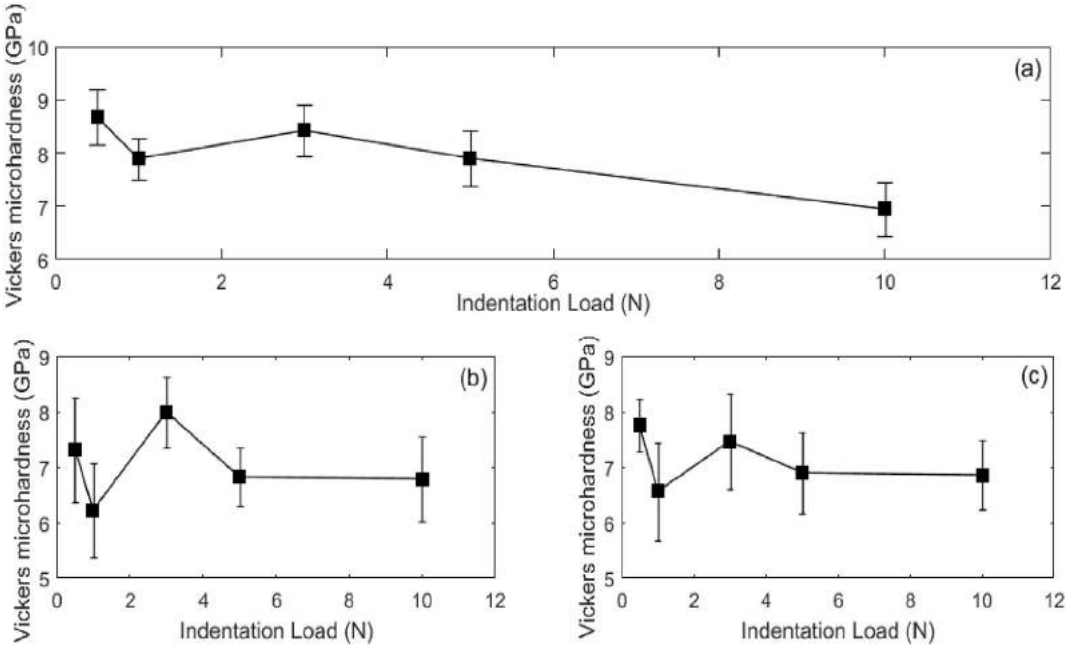


**Fig. 8.** The Vickers microhardness as a function of the applied indentation load for (a) A0.2, (b) A0.3 and (c) A0.4 samples.

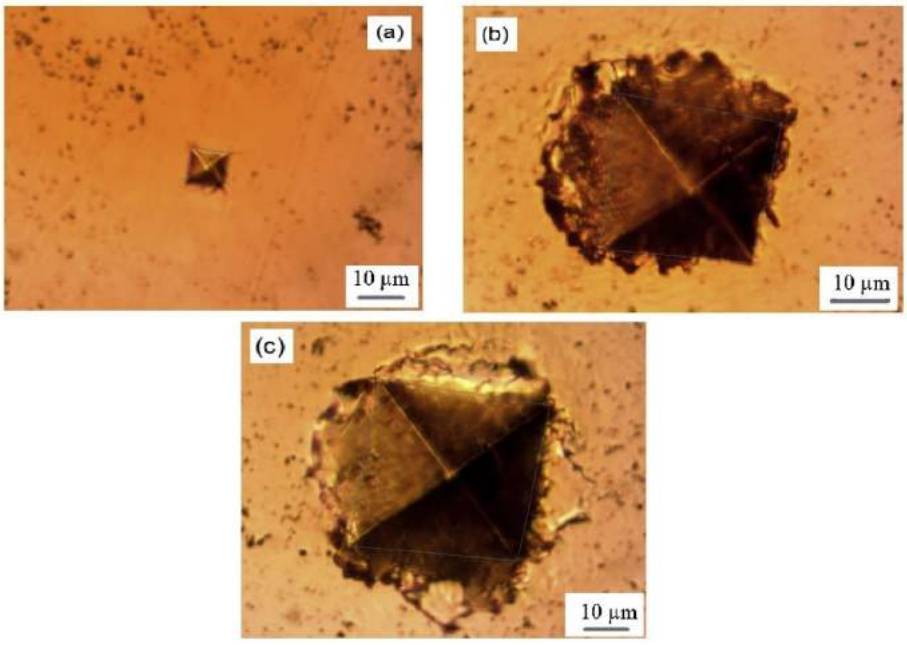


**Fig. 9.** Optical micrographs of Vickers indentation conducted on A0.2 sample at the loads of (a) 0.5, (b) 5 and (c) 10 N.

**Table 6**
The results of the longitudinal sound velocity and the Young's modulus of A0.1, A0.2, A0.3 and A0.4 samples.

| Sample | A0.1 | A0.2 | A0.3 | A0.4 |
|---|---|---|---|---|
| Longitudinal sound velocity ($m.s^{-1}$) | 7985.5 | 9314.33 | 9323.66 | 9328.87 |
| Young's modulus (GPa) | 235.02 | 346.46 | 347.81 | 348.92 |

sound velocity and Young's modulus was diminished. The specific stiffness ($E/\rho$) of high-purity $Ti_3SiC_2$ samples ($\approx$78 GPa $cm^3$ $g^{-1}$) was very close to $Si_3N_4$ one which is higher than many metal and ceramic compounds [5].

## 4. Conclusion

High-purity single-phase $Ti_3SiC_2$ samples were synthesized by spark plasma sintering of Ti:Si:TiC:Al = 1:1:1.2:x (0.2–0.4) at the sintering temperature of 1150 °C under unidirectional pressure of 40 MPa for 8 min. Appropriate addition of Al enhanced the densification process and decreased both initiation and completion temperatures of densification. Moreover, the addition of Al decreased the optimum sintering temperature. With decreasing the Al content, $Ti_3SiC_2$ was formed besides TiC and $Ti_5Si_3$ phases as auxiliary phases. The Rietveld refinement and standard additive method used to determine the weight percentage of $Ti_3SiC_2$, TiC and $Ti_5Si_3$ phases, led to obtaining different results which was caused by many and strongly overlapping peaks. The Vickers microhardness values of high-purity $Ti_3SiC_2$ samples were determined $\approx$6.8 GPa at 10 N load. The highest Young's modulus was about 349 GPa and decreased with lowering Al content and density.

## References

[1] M.W. Barsoum, T. El-Raghy, Synthesis and characterization of a remarkable ceramic: Ti=$SiC_2$, J. Am. Ceram. Soc. 79 (1996) 1953–1956.
[2] M.W. Barsoum, T. El-Raghy, The MAX phases: unique new carbide and nitride materials, Am. Sci. 89 (2001) 334–343.
[3] T. El-Raghy, A. Zavaliangos, M.W. Barsoum, S.R. Kalidindi, Damage mechanisms around hardness indentations in $Ti_3SiC_2$, J. Am. Ceram. Soc. 80 (1997) 513–516.
[4] X.K. Qian, Methods of MAX-phase synthesis and densification – I, in: Advances in Science and Technology of $M_{n+1}AX_n$ Pahses, Xi'an University of Architecture and Technology, Woodhead Publishing, P.R. China, 2012, pp. 1–19.
[5] M.W. Barsoum, MAX Phases: Properties of Machinable Ternary Carbides and Nitrides, Wiley-VCH Verlag GmbH & Co. KGaA, Weinheim, Germany, 2013.
[6] J. Lis, Y. Miyamoto, R. Pampuch, K. Tanihata, $Ti_3SiC_2$-Based materials prepared by HIP-SHS techniques, Mater. Lett. 22 (1995) 163–168.
[7] R. Pampuch, J. Lis, J. Piekarczyk, L. Stobierski, $Ti_3SiC_2$-Based materials produced by self-propagating high-temperature synthesis (SHS) and ceramic processing, J. Mater. Synth. Process. 1 (1993) 93.
[8] M.W. Barsoum, M. Radovic, Elastic and mechanical properties of the MAX phases, Annu. Rev. Mater. Res. 41 (2011) 195–227.
[9] M.W. Barsoum, The $M_{N+1}AX_N$ phases: a new class of solids, Prog. Solid State Chem. 28 (2000) 201–281.
[10] T. El-Raghy, M.W. Barsoum, Processing and mechanical properties of $Ti_3SiC_2$: reaction path and microstructure evolution, J. Am. Ceram. Soc. 82 (1999) 2849–2854.
[11] N.F. Gao, Y. Miyamoto, K. Tanihata, Dense $Ti_3SiC_2$ prepared by reactive HIP, J. Mater. Sci. 34 (1999) 4385–4392.
[12] R. Radhakrishnan, J.J. Williams, M. Akinc, Synthesis and high-temperature stability of $Ti_3SiC_2$, J. Alloys Compd. 285 (1999) 85–88.
[13] J.Q. Zhu, B.C. Mei, X.W. Xu, J. Liu, Synthesis of single-phase polycrystalline $Ti_3SiC_2$ and $Ti_3AlC_2$ by hot pressing with the assistance of metallic Al or Si, Mater. Lett. 58 (2004) 588–592.
[14] L. Cui-Ying, Y. Xiao-Wei, L. Xiang-Ming, A novel in-situ synthesis route of $Ti_3SiC_2$-SiC composite by liquid silicon infiltration, J. Inorg. Mater. 25 (2010) 1003–1008.
[15] S.S. Hwang, J. Han, D. Lee, S.W. Park, Synthesis of $Ti_3SiC_2$ by infiltration of molten Si, J. Alloys Compd. 509 (2011) 336–339.
[16] H. Foratirad, H.R. Baharvandi, M. Ghanadi Maraghe, Effect of excess silicon content on the formation of nano-layered $Ti_3SiC_2$ ceramic via infiltration of TiC preforms, J. Eur. Ceram. Soc. 37 (2017) 451–457.
[17] H. Foratirad, H.R. Baharvandi, M. Ghanadi Maragheh, Synthesis of nanolayered $Ti_3SiC_2$ MAX phase via infiltration of porous TiC preform produced by the gelcasting process, Mater. Lett. 180 (2016) 219–222.
[18] H. Li, L.M. Peng, M. Gong, J.H. Zhao, L.H. He, Effect of Al addition on synthesis of the $Ti_3SiC_2$ by vacuum sintering, Z. für Phys. Chem. 219 (2005) 1411–1420.
[19] N.F. Gao, J.T. Li, D. Zhang, Y. Miyamoto, Rapid synthesis of dense $Ti_3SiC_2$ by spark plasma sintering, J. Eur. Ceram. Soc. 22 (2002) 2365–2370.
[20] J.Q. Zhu, B.C. Mei, Effect of aluminum on synthesis of $Ti_3SiC_2$ by spark plasma sintering (SPS) from elemental powders, J. Mater. Synth. Process. 10 (2002) 353–358.
[21] C.F. Hu, Y. Sakka, S. Grasso, H. Tanaka, T. Nishimura, Spark plasma sintering (SPS), or pulse discharge sintering (PDS) of MAX phases, in: MAX Phases: Microstructure, Properties, and Applications, Nova Science Publishers Inc., New York, 2012.
[22] N.C. Ghosh, S.P. Harimkar, Consolidation and synthesis of MAX-phases by

spark plasma sintering (SPS): a review, in: Advances in Science and Technology of $M_{n+1}AX_n$ Pahses, Oklahama State University, Woodhead Publishing, USA, 2012, pp. 47–80.
[23] Z.F. Zhang, Z.M. Sun, H. Hashimoto, T. Abe, Application of pulse discharge sintering (PDS) technique to rapid synthesis of $Ti_3SiC_2$ from Ti/Si/C powders, J. Eur. Ceram. Soc. 22 (2002) 2957–2961.
[24] Z.M. Sun, Z.F. Zhang, H. Hashimoto, T. Abe, Ternary compound $Ti_3SiC_2$: Part I. Pulse discharge sintering synthesis, Mater. Trans. 43 (2002) 428–431.
[25] J.Q. Zhu, B.C. Mei, Fabrication of high-purity $Ti_3SiC_2$ by spark plasma sintering (SPS) of elemental powders, J. Mater. Sci. Lett. 22 (2003) 889–890.
[26] W.B. Zhou, B.C. Mei, J.Q. Zhu, Fabrication of high-purity ternary carbide $Ti_3SiC_2$ by spark plasma sintering technique, Mater. Lett. 59 (2005) 1547–1551.
[27] Z.F. Zhang, Z.M. Sun, H. Hashimoto, Rapid synthesis of ternary carbide $Ti_3SiC_2$ through pulse-discharge sintering technique from Ti/Si/TiC powders, Metall. Mater. Trans. A 33 (2002) 3321–3328.
[28] Z.F. Zhang, Z.M. Sun, H. Hashimoto, Low temperature synthesis of $Ti_3SiC_2$ from Ti/SiC/C powders, Mater. Sci. Technol. 20 (2004) 1252–1256.
[29] Z.F. Zhang, Z.M. Sun, H. Hashimoto, T. Abe, A new synthesis reaction of $Ti_3SiC_2$ through pulse discharge sintering Ti/SiC/TiC powder, Scr. Mater. 45 (2001) 1461–1467.
[30] Z.F. Zhang, Z.M. Sun, H. Hashimoto, T. Abe, A new synthesis reaction of $Ti_3SiC_2$ from Ti/TiSi2/TiC powder mixtures through pulse discharge sintering (PDS) technique, Mater. Res. Innov. 5 (2002) 185–189.
[31] Y. Zou, Z.M. Sun, S. Tada, H. Hashimoto, Synthesis reactions for $Ti_3SiC_2$ through pulse discharge sintering TiH2/Si/TiC powder mixture, Mater. Res. Bull. 43 (2008) 968–975.
[32] F. Turki, H. Abderrazak, F. Schoenstein, M. Abdellaoui, N. Jouini, SPS parameters influence on $Ti_3SiC_2$ formation from Si/TiC: mechanical properties of the bulk materials, J. Alloys Compd. 708 (2017) 123–133.
[33] N.C. Ghosh, S.P. Harimkar, Microstructure and wear behavior of spark plasma sintered $Ti_3SiC_2$ and $Ti_3SiC_2$–TiC composites, Ceram. Int. 39 (2013) 4597–4607.
[34] J. Zhang, L. Wang, W. Jiang, L. Chen, Fabrication of high purity $Ti_3SiC_2$ from Ti/Si/C with the aids of Al by spark plasma sintering, J. Alloys Compd. 437 (2007) 203–207.
[35] H. Gao, R. Benitez, W. Son, R. Arroyave, M. Radovic, Structural, physical and mechanical properties of $Ti_3(Al_{1-x}Si_x)C_2$ solid solution with x=0–1, Mater. Sci. Eng. A 676 (2016) 197–208.
[36] H.M. Rietveld, A profile refinement method for nuclear and magnetic structures, J. Appl. Crystallogr. 2 (1969) 65–71.
[37] M.J. Assael, K. Kakosimos, R.M. Banish, J. Brillo, E. Egry, R. Brooks, P.N. Quested, K.C. Mills, A. Nagashima, Reference data for the density and viscosity of liquid aluminum and liquid iron, J. Phys. Chem. Ref. Data 35 (2006) 286–300.
[38] A.T. Dinsdale, P.N. Quested, The viscosity of aluminium and its alloys—a review of data and models, J. Mater. Sci. 39 (2004) 7221–7228.
[39] K.Y. Xie, M.F. Toksoy, K. Kuwelkar, B. Zhang, J.A. Krogstad, R.A. Haber, K.J. Hemker, Effect of alumina on the structure and mechanical properties of spark plasma sintered boron carbide, J. Am. Ceram. Soc. 97 (2014) 3710–3718.
[40] Ch. Xu, Y. Cai, K. Flodström, Zh. Li, S. Esmaeilzadeh, G.J. Zhang, Spark plasma sintering of $B_4C$ ceramics: the effects of milling medium and $TiB_2$ addition, Int. J. Refract. Met. Hard Mater. 30 (2012) 139–144.
[41] N.C. Ghosh, S.P. Harimkar, Phase analysis and wear behavior of in-situ spark plasma sintered $Ti_3SiC_2$, Ceram. Int. 39 (2013) 6777–6786.
[42] D. Lu, Y. Yang, Y. Qin, G. Yang, Effect of particle size and sintering temperature on densification during coupled multifield-activated microforming, J. Mater. Res. 27 (2012) 2579–2586.
[43] B. Yavas, F. Sahin, O. Yucel, G. Goller, Effect of particle size, heating rate and CNT addition on densification, microstructure and mechanical properties of $B_4C$ ceramics, Ceram. Int. 41 (2015) 8936–8944.
[44] R.W. Rice, Hardness-grain-size relations in ceramics, J. Am. Ceram. Soc. 77 (1994) 2539–2553.
[45] Y.C. Zhou, J.X. Chen, J.Y. Wang, Strengthening of $Ti_3AlC_2$ by incorporation of Si to form $Ti_3Al_{1-x}Si_xC_2$ solid solutions, Acta Mater. 54 (2006) 1317–1322.
[46] T. Goto, T. Hirai, Chemically vapor deposited $Ti_3SiC_2$, Mater. Res. Bull. 22 (1987) 1195–1201.
[47] H.O. Pierson, Handbook of Refractory Carbides and Nitrides, Noyes Publications, Westwood, NJ, 1996.
[48] H. Abderrazak, F. Turki, F. Schoenstein, M. Abdellaoui, N. Jouini, Effect of the mechanical alloying on the $Ti_3SiC_2$ formation by spark plasma sintering from Ti/Si/C powders, Int. J. Refract. Met. Hard Mater. 35 (2012) 163–169.
[49] P. Finkel, M.W. Barsoum, T. El-Raghy, Low temperature dependencies of the elastic properties of $Ti_4AlN_3$, $Ti_3Al_{1.1}C_{1.8}$, and $Ti_3SiC_2$, J. Appl. Phys. 87 (2000) 1701–1703.
[50] M. Radovic, M.W. Barsoum, A. Ganguly, T. Zhen, P. Finkel, S.R. Kalidindi, E. Lara-Curzio, On the elastic properties and mechanical damping of $Ti_3SiC_2$, $Ti_3GeC_2$, $Ti_3Si_{0.5}Al_{0.5}C_2$ and $Ti_2AlC$ in the 300–1573 K temperature range, Acta Mater. 54 (2006) 2757–2767.